Composite layup effect on the failure mechanism of single lap bonded joints

Kupski, J.; Teixeira de Freitas, S.; Zarouchas, D.; Camanho, P. P.; Benedictus, R.

DOI
10.1016/j.compstruct.2019.02.093

Publication date
2019

Document Version
Final published version

Published in
Composite Structures

Composite Structures 217 (2019) 14–26

Contents lists available at ScienceDirect

Composite Structures

journal homepage: www.elsevier.com/locate/compstruct

Composite layup effect on the failure mechanism of single lap bonded joints

J. Kupski[a], S. Teixeira de Freitas[a,*], D. Zarouchas[a], P.P. Camanho[b,c], R. Benedictus[a]

[a] Structural Integrity & Composites Group, Delft University of Technology, Kluyverweg 1, 2629HS, Netherlands
[b] DEMEC, Faculdade de Engenharia, Universidade do Porto, Rua Dr. Roberto Frias, 4200-465 Porto, Portugal
[c] INEGI, Rua Dr. Roberto Frias, 400, 4200-465 Porto, Portugal

ARTICLE INFO

Keywords:
Composite bonded joints
Single lap joints
Composite layup variation

ABSTRACT

Single lap bonded joints with four different composite adherend stacking sequences were tested and numerically simulated. The aim was to evaluate the effect of the layups on the quasi-static tensile failure of the bonded joints. The study shows that increasing the adherends bending stiffness postpones the damage initiation in the joint. However, this is no longer valid for final failure. The ultimate load is influenced by how the damage progresses. For similar bending stiffness, a layup that leads to the crack propagating from the adhesive towards the inside layers of the composite increases the ultimate load. The failure mode is highly influenced by the orientation of the interface lamina in contact with the adhesive, such that, a 0° interface ply causes failure within the bond line, while a 90° interface ply causes failure inside the composite adherend.

Finally, it is concluded that a quasi-isotropic layup may not be the best choice in terms of tensile joint strength. In order to improve tensile strength up to damage initiation, the layup should be optimized for bending stiffness, while up to final failure, a stacking sequence that yields to a complex crack path inside the composite can lead to higher ultimate loads.

1. Introduction

With the recent launch of the Boeing 787 Dreamliner and the Airbus A350 XWB, airplane fuselage structures made out of Carbon Fibre Reinforced Plastic (CFRP) were introduced in civil aviation. However, besides outstanding strength and stiffness-to-weight ratios along the fibre direction, CFRPs often show low mechanical properties, such as elastic moduli and strength, in the transverse and through-thickness direction [1–3]. Thus, when using CFRP adherends in joint topologies that induce high peel stresses in the thickness direction, such as Single Overlap Joints (SLJ) and skin-to-stiffener joints, the resultant ultimate joint strength, associated to inter- and intra-laminar failure of the composite, is much lower than the same topologies using metal adherends, which fail entirely in the bond line [3,4]. This drawback in using CFRP is hindering their performance and efficiency in full-scale structures where joints are essential.

Today's standard CFRP layups used in large aerospace structures are quasi-isotropic, such as $[(45/90/-45/0)_2]_s$ [5]. This choice is mainly tied to the easiness of manufacturing and to composite design rules used by industry (e.g. 10%-rule) [6]. However, latest developments in manufacturing techniques allow for a wider choice of CFRP layups. As an example, the fuselage of the A350 XWB is being built by Automated Fibre Placement (AFP) techniques. By changing the laminate stacking sequence, composite properties can be optimized towards the external loading. Research in the field of composites shows that certain stacking sequences can retard delamination [7–9]. Therefore making use of the composite's anisotropy could potentially counteract their poor out-of-plane strength, which can have a positive impact on the performance of composite adhesively bonded joints subject to peel stresses.

Furthermore, literature has explored other promising improvements in terms of enhancing joint strength under tensile loading, for example by application of a high toughness resin in combination with a ductile thermoplastic interlayer on the adherend-adhesive interface [10,11]. However, the focus of this paper is particularly on the design parameter ''layup'', without taking into account any other method to increase the joint strength.

Various studies on different layups for adhesively bonded CFRP-SLJs have been performed since 1973. L. J. Hart-Smith [12] developed an iterative closed-form elasto-plastic analytical solution to determine the stress field distribution along SLJs. He used this approach to study the influence of laminate bending stiffness on the stress distribution along the overlap. His results show an increase in joint efficiency ($\sigma_{avg}/\sigma_{max}$) for laminates with 0° layers concentrated near the outer faces when compared to laminates with 0° layers close to the neutral axis. The reason why stiff laminates lead to higher efficiencies is, that a high bending stiffness of the adherend reduces their bending curvature and

* Corresponding author.
E-mail address: s.teixeiradefreitas@tudelft.nl (S. Teixeira de Freitas).

https://doi.org/10.1016/j.compstruct.2019.02.093
Received 30 December 2018; Received in revised form 21 February 2019; Accepted 22 February 2019
Available online 23 February 2019

therefore stiff laminates experience less severe peel stresses than more flexible adherends. This trend was noticed both for balanced and unbalanced laminates and for various overlap lengths. Two years after, Renton et al. [13] reveal a similar trend. By also using an analytical approach to determine the stress distribution along the overlap, they conclude that, for maximizing the static and fatigue load carrying capability of an adhesively bonded joint, the edge shear and moment concentrations at the ends of the overlap and the peak adhesive shear and normal stresses should be minimized. By reducing the peak adhesive stresses, the shear stress distribution in the adhesive becomes more uniform and the normal transverse (peel) stress, especially at the joint edges, reduces to insignificant values. To achieve this, it is recommended to use adherends with high bending stiffness. It is further noted that, for certain geometries of laminated adherends, the large tensile and compressive longitudinal stresses near the ends of the overlap in combination with the peak transverse shear and peel stresses are responsible for a composite failure instead of a failure in the bond line. To avoid failure of the composite adherend, it is recommended to orient the plies of the laminates to small angles, increasing the bending stiffness and resulting in smother stress distributions in the adherend. More recently, Aydin [14] expanded this research by establishing a 3D non-linear finite element model to evaluate the effect of ply angle on the stress distribution and initial damage prediction in SLJs under uniaxial tensile loading. His work concludes that the state of stress in the vicinity of the free edge of the joint is 3-dimensional and that neglecting the out-of-plane stress distributions would result in inaccurate static strength predictions in the analysis of composite bonded joints. He further concludes that, an increasing number of 0° layers leads to lower stress distribution in the SJL due to the increased longitudinal bending stiffness of the adherends, which is in agreement with previous studies. The numerical and experimental studies of Ozel et al. [15] showed, that CFRP adherends with different stacking sequences, adherend thicknesses and overlap lengths affect significantly the failure load and stress distribution in the SLJ. The results show that, the load carrying capacity of joints with a layup of $[0/45/-45/90]_4$ increased by 48%, 62% and 123% when compared to $[0]_{16}$, $[0/90]_8$, and $[45/-45]_8$, respectively. This study shows the significance and the potential of the composite laminate design to the performance of SLJs. Khan et al. [16] studied the influence of the stacking sequence on the failure mode of composite Double Lap Joints (DLJs). Based on an experimental campaign, it is concluded that the maximum joint performance is associated with specimens exhibiting cohesive failure, whereas minimum joint performance is associated with intraply/interfacial failure. Moreover, the percentage of intraply failure increased when the ply in contact with the adhesive was oriented 90°. Purimpat et al. [17] performed extensive experimental studies on the effect of fibre angle orientation of single lap joints with quasi-static/quasi-homogeneous layups, using epoxy paste adhesive. The study goes further on the effect of the 0° layer, stating that, the failure strength is dependent not only on the global properties of the laminates but also on the local orientations of the laminates. The test performed show, that if the stiffness properties are maintained constant, larger angles close to the bond line result in more complex crack paths and can increase the joint strength by 30%. Meneghetti et al. [18,19] showed a similar trend when studying the influence of the interface ply orientation on the fatigue behaviour of bonded CFRP-SLJs. Their experimental results indicate that a 45° ply at the adhesive-composite interface significantly increases the resistance to crack propagation. It is also reported, though, that in comparison with changes in geometry, such as corner shape at the end of the bonded area and overlap length, a change in layer orientation at the adhesive-adherend interface was less effective to increase the fatigue strength.

A comparison of previous studies depicts a general agreement: increasing the SLJ's longitudinal bending stiffness, either by increasing the number of 0° layers or by placing those near the outside faces of the adherends, results in a reduction of peel stresses at the tips of the bond line and increases the overall joint strength under tensile loading. However, there is no common agreement on the most beneficial layup sequence to increase the load at damage initiation compared to one at maximum failure load. While some studies indicated that 0° layer close to the interface with the adhesive will lead to higher load strength [12–16], other studies give contradictory indications, stating that larger angles will increase the joint strength [17–19]. This also leads to paradoxical results in terms of the most beneficial failure mode, along with the highest joint strength (if there is any consistency): some studies claim cohesive failure leads to higher strengths [16] while other show benefits in the more complex intraply failure to the joint strength [17]. In-plane longitudinal bending stiffness may be the most relevant design parameter to decrease peak peel stresses, which correlates with a 0° ply orientation adjacent to the bond line interface and subsequently a cohesive failure inside the adhesive material. But this choice may only be valid until damage initiation. At final failure, the situation might differ. The missing piece is therefore, to analyse the failure modes of lap joints with various layups and to record the corresponding load at damage initiation, as well as the maximum load, in order to address those discrepancies. An implementation into a 3D finite element model would then give insight into the stress field around the bond line and would help explain the failure mechanisms. At the end, the question could be addressed, whether an optimized layup (for the specific CFRP bonded SLJ design and material of choice) should or should not have a 0° layer adjacent to the bond line and why the appearance of this particular fibre orientation seems to always prevent a crack to grow further into the composite. This work aims exactly to address the above mentioned questions and give more insight into the effect of the layup of the laminate on the damage initiation and final failure of composite SLJs. Adhesively bonded SLJs made from CFRP adherends with different layups and epoxy film adhesive are analysed experimentally and numerically. The case study is narrowed to primary aircraft fuselage panels as potential application for bonded joints. However, the methodology may also be applied in other fields where material properties and design requirements differ.

2. Materials and specimens

2.1. Materials

The materials used for this study are unidirectional Prepreg tapes from carbon fibres and epoxy resin in combination with an epoxy film adhesive. The Prepreg tape is Hexply® F6376C-HTS(12K)-5-35% (Hexcel Composites in Duxford, UK), containing high tenacity Tenax®-E HTS45 standard modulus fibres (Toho Tenax Europe GmbH) and the Hexply® F6376 thermoplastic-toughened epoxy matrix system. The adhesive was chosen Hysol® EA 9695™ 050K AERO in 240 g/m^2 areal weight, including a knit supporting carrier (Henkel AG & Co. KGaA in Duesseldorf, Germany). The relevant material parameters, extracted from material datasheet [20], as well as from previous studies with similar adhesives [4,21], are presented in Tables 1 and 2. All values are valid at room temperature (23 °C). Indices are given for different coordinate directions with "1", "2" and "3" standing for the direction along in-plane longitudinal, in-plane transverse and out-of-plane, and with "T" and "C" standing for "tensile" and "compressive", respectively.

2.2. Specimens

Specimens were built according to the ASTM standard D 5868-01 [22], with a constant overlap length and width of 25.4 mm. The composite adherends consist of 16 UD-layers of 0.125 mm single ply thickness. Table 3 lists the four different layups investigated with their correspondent longitudinal bending stiffness. The reference fuselage panel is represented by the quasi-isotropic stacking sequence $[(45/90/-45/0)_2]_s$, with 45° as the outermost layer in contact with the adhesive. The two other configurations are also quasi-isotropic, with 90°

Table 1
Material properties of Hexply® 6376C-HTS(12K)-5-35% for a UD-Prepreg layer [20].

Longitudinal tensile strength	X_T	2274 MPa
Longitudinal compressive strength	X_C	1849 MPa
Transverse tensile strength	Y_T	102 MPa
Transverse compressive strength	Y_C	255 MPa
Longitudinal tensile modulus	E_{11T}	142,000 MPa
Transverse tensile modulus	$E_{22T} = E_{33T}$	9100 MPa
In-plane shear modulus	$G_{12} = G_{13}$	5200 MPa
Transverse shear modulus	$G_{23} = E_{33T}/(2(1 + \nu_{23}))$	3500 MPa
In-plane shear strength	$S_{12} = S_{13}$	63 MPa
Transverse shear strength	S_{23}	35 MPa
In-plane Poisson ratio	$\nu_{12} = \nu_{13}$	0.27
Transverse Poisson ratio	ν_{23}	0.30

Table 2
Adhesive material properties, [a]from previous studies adopted to Hysol® EA 9695™ 050K AERO and [b]from TDS [4,21].

Tensile strength	X_{Adh}	48 MPa[a]
Maximum elongation at break	ε_{tmax}	11.5 %[a]
Tensile modulus	E_{Adh}	2019 MPa[a]
Poisson ratio	ν_{adh}	0.34[b]

Table 3
Layup configurations.

Stacking sequence	Equivalent longitudinal bending stiffness
$[(45/90/-45/0)_2]_s$	39.6 GPa
$[(90/45/0/-45)_2]_s$	46.0 GPa
$[(0/45/90/-45)_2]_s$	72.4 GPa
$[(45/0/-45/0)_2]_s$	69.4 GPa

and 0° as the outermost layer, respectively. By comparing these three layups, the effect of the fibre angle in contact with the adhesive layer will be studied. The fourth configuration maintains the outer layer of 45° as in the reference but with higher number of 0° layers. In this way, a comparison with the reference layup will show the effect of increasing the longitudinal bending stiffness without changing the fibre angle in contact with the adhesive layer (45° on both).

The longitudinal bending stiffness was determined based on the classical laminate theory as the flexural engineering constant of a laminate given by

$$E_x^f = \frac{12}{D_{11}^* t^3} \quad (1)$$

for symmetric layups, where D^*_{11} is the corresponding first row/first column entry of the resulting inverse of the bending stiffness matrix, t is the overall laminate thickness of 2 mm and x corresponds to the direction along the SLJ-length (longitudinal direction) [23].

2.3. Laminating process

The adherends were laminated in a Prepreg hand layup process, with 20 min of debulking at an under pressure lower than 100 mbar in between every second layer. All laminates were cured in the same cycle, packed between a base and a caul plate from aluminium. Fiberflon® 408.07-P PTFE coated glass fabric was used in the laminate surface to be bonded instead of conventional silicone coated peel ply. This is in accordance with the recommendation from literature in which the Fiberflon® 408.07-P PTFE coated glass fabric was the only peel ply out of five tested that obtained good adhesion after peel ply removal [24].

The autoclave curing cycle for the Hexply® 6376C-HTS(12K)-5-35% Prepreg laminate, was at 180 °C and 9 bar gauge pressure for 120 min time. The setup resulted in plates with a roughness of 60 µm average depth on both surfaces. This roughness has been measured using a Olympus LEXT OLS3100 confocal laser scanning microscope, on a remaining piece of one of the original Prepreg plates. The measurement was performed at the outside of the plate, within the last ca. 50 mm from the edge of the plate. It was ensured that the focus of the laser scan was not chosen too close to the edge of the specimen, where apparent delamination due to rough mechanical trimming may give a misleading result.

2.4. Surface treatment

A suitable surface treatment prior to bonding was chosen as combination of degreasing the surface with Acetone and UV/ozone treatment. The UV/Ozone treatment is a physical treatment consisting of the application of high intensity ultra violet light in the presence of ozone gas to both clean and modify the surface of the specimen on a molecular level. This treatment is effective for the removal of organic contaminants. The process works by decomposing the organic compounds into volatile substances (i.e. water and carbon dioxide) with the use of ultraviolet rays (important wave lengths for this process are 184.9 nm to 253.7 nm) and by strong oxidations during the formation and decomposition of the ozone [25,26]. However, the use of UV/ozone is ineffective for removing inorganic contaminants. Therefore, the surface was previously cleaned with acetone, to remove the bulk of organic contaminants and the inorganic surface contaminants that may be present. The UV/ozone treatment was applied for 7 min, with the UV-light tubes distancing 40 mm from the specimen surface. Bonding the adherends was performed within 30 min after the application of the surface treatment. This procedure was performed according to previous studies that showed good CFRP surface wettability after applying the same method [27].

2.5. Bonding process

The adhesive bonding process was performed by laying the uncured film adhesive onto the cured adherends and arranging a vacuum setup around them. Fig. 1 shows the dimensions of the SLJs and a picture of the final specimens. The SLJs dimensions are in accordance with standard ASTM D 5868-01 [22].

Excess adhesive gathered at the bond line tips and formed a small fillet at the edges – Fig. 1b). The curing process was performed in an autoclave at 2 bar gauge pressure and 177 °C curing temperature for 120 min dwell time.

2.6. Reduced bond line thickness

After bonding, the adhesive thickness of each specimen was measured by taking from the total overlap thickness, the total thickness of both CFRP adherends. The final adhesive thickness was significantly smaller than the recommended value between 150 µm and 200 µm, according to the material datasheet, revealing a mean value of 44 ± 47 µm. Adhesive flow out due to over pressure in the curing phase would be a possible explanation for such a reduced thickness. However, lots of care has been taken by adjusting the adhesive bonding cycle. After a series of curing pre-trials, both with different temperature and pressure values, as well as after contacting the manufacturer about this issue, a cycle of 2 h steady hold at 177 °C at a relative over pressure of 2 bar was identified as best compromise for excess squeeze out versus the prevention of voids. It is therefore believed, that the significant roughness of both adherend surfaces (60 µm), adjacent to the bond line, may have soaked a major portion of the adhesive material into their cavities and caused the reduced bond line thickness.

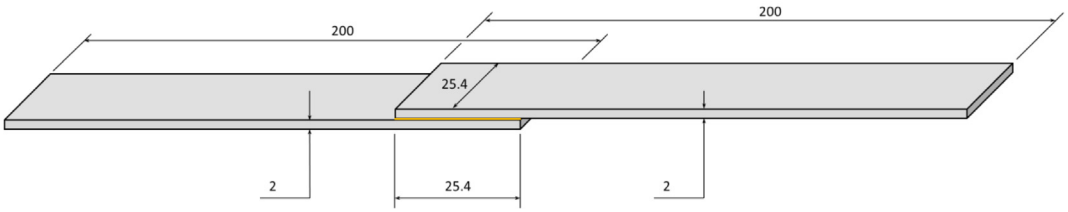

a) SLJ specimen design (dimensions in mm)

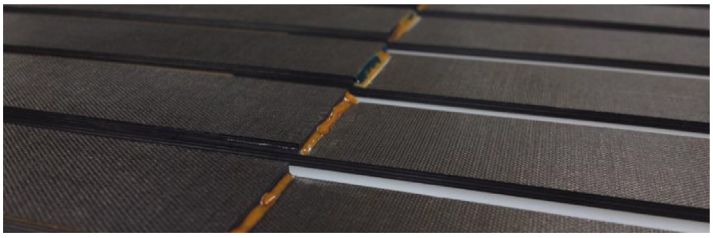

b) Picture of the specimens

Fig. 1. Single Lap bonded Joints.

3. Experimental methods

3.1. Surface analysis

A surface analysis using contact angle measurements was performed to the treated CFRP surfaces to assess their wettability. The contact angle of a 4 µl distilled water drop was measured for the rough specimen surface, having a topology imprint from the PTFE/glass fabric with 60 µm surface roughness, using the Technex Cam200/Attension Theta V4.1.9.8 system.

3.2. Quasi-static tensile tests

Five specimens per layup configuration were subject to quasi-static tensile loading in accordance to ASTM standard D 5868-01 [22]. The tests were displacement controlled with a constant displacement rate of 1.3 mm/min. They were performed on a Zwick-Roell AllroundLine Z250 SW testing machine with a load cell of 250 kN. Fig. 2 illustrates a schematic representation of the test setup. The specimen was hold by two clamps at 250 bar hydraulic pressure. The initial distance of the clamps was set at 200 mm, with a misalignment of 2 mm to counterbalance the overlap offset. A mechanical extensometer, BTC-EX-MACRO.H02 by Zwick-Roell/testXpert II, captured the elongation between two points of 60 mm distance, adjacent to the overlap area. Additionally, the strain field of the overlap area was monitored using digital image correlation (DIC) technique. For this, the VIC-3D™ system by Correlated Solutions, Inc. was used at a 2 Hz frame capture speed. In order to monitor the damage initiation of the specimens, an acoustic emission (AE) system by Vallen Systeme GmbH was employed, consisting of two VS900-M sensors, which were attached onto the same side of the specimen at ± 42.5 mm from the overlap centre and connected to the AEP4H 34 dB amplifier.

4. Numerical analysis

A finite element analysis (FEA) was performed with the commercial software Abaqus, V6.14-1. The purpose of the FEA was to numerically simulate the SLJ under tensile loading. An implementation into a 3D-model gives insight into the stress field around the bond line, aiming to interpret the resulting failure mechanisms. The composite was modelled as linear elastic, based on the properties listed in Table 1, while the adhesive was modelled linear-elastic/plastic, using those values from Table 2. The load was applied in a single step with 6 load increments taking into account non-linear geometry effects.

The specimen between the clamps was simulated using solid 3D-elements. Fig. 3 illustrates the model, including dimensions, boundary conditions and mesh. At the right side all 6 Degrees of Freedom (DoF) are fixed, while on the left side, solely longitudinal displacement is allowed (x-direction). Although the average bond line thickness in the real specimens was 44 µm (± 47 µm), it was decided to model the bond line thickness as 62.5 µm. This value is the upper limit of the adhesive thickness measured at the real specimens instead of the average bond line thickness and it was considered to be a good compromise between real specimen dimensions and numerically feasible.

In Fig. 4 the region around the left overlap edge is illustrated. The spew fillet dimensions are a representation of what was measured in the real specimens. All 4 × 5 specimen of this study had a spew fillet shape similar to a 45° triangle. In fact, the shape was in 16 cases rather

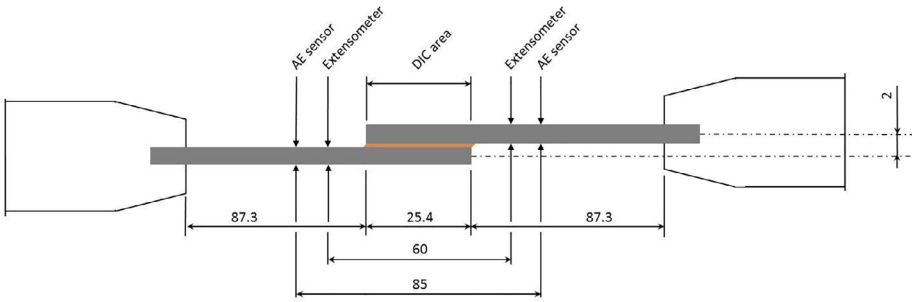

Fig. 2. Test setup for static tensile loading (dimensions in mm).

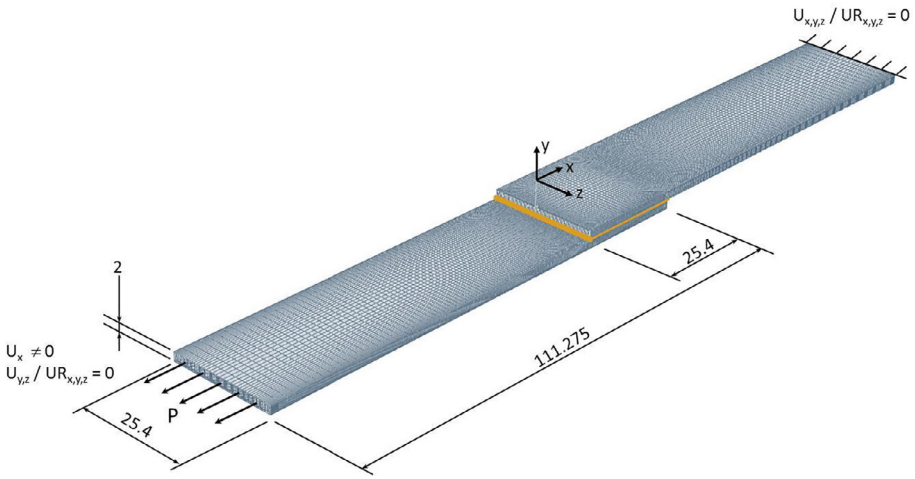

Fig. 3. 3D FE-model between the clamps with specimen dimensions and boundary conditions (dimensions in mm).

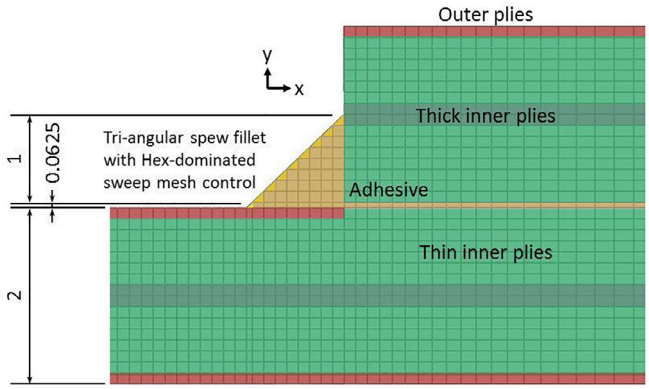

Fig. 4. Zoom on fillet region and material section assignments (dimensions in mm).

convex, and in 4 cases concave. For 8 specimen, the height of the spew fillet reached all the way up to the top of the adherends, while in the remaining cases developing less volume. However, in all cases, the spew fillet reached at least up to half of the adherend's height (=1 mm). Based on this, it was decided to model a triangular fillet shape of 45° slope reaching up half the adherend's height, as a good approximation to represent the specimens within this study.

Each composite adherend is modelled with 16 elements through the total thickness of 2 mm, which corresponds to one element per single UD-layer of 125 µm. Amongst different element types, offered by Abaqus, V6.14-1 Implicit, the linear 3D-continuum element with 8 nodes (C3D8) has been selected for a feasible numerical accuracy versus computational cost for the specific boundary conditions and dimensions of the SLJ-design. The mesh density of the model has been refined along the overlap length of the joint to gain numerical accuracy at regions with stress concentrations.

A mesh convergence study has been performed in order to guarantee that the results were mesh independent. In Fig. 5, the peel stress (σ_{yy}) is plotted along the overlap length, from left to right, including the length of both fillets in Fig. 5a), and through the thickness of the overlap left edge, from bottom to top in Fig. 5b). Both paths are situated in the centre of the joint in width direction. In order to avoid stress singularities at any interface, the path in Fig. 5a) was chosen exactly in the middle of the bond line and in Fig. 5b) 31.25 µm inwards of the overlap end (in x-direction). The length and height of one element in this overlap tip region is set to 125 µm, so that the path was plotted at ½ of an element thickness in Fig. 5a) and at ¼ of an element length in Fig. 5b).

The dimensions of Mesh 1 in Fig. 5a) were based on the smallest element size at the bond line region with the dimensions length = 125 µm, height = 62.5 µm, width = 500 µm, leading to 688,296 elements in total. A mesh refinement has been performed increasing the number of elements in the overlap region and leading to a total number of 732054 (Mesh 2). A sufficient convergence in stress values could be established with the coarser Mesh 1 of 688296 elements of type C3D8. All the results presented in this paper are therefore based on Mesh 1.

5. Experimental results

5.1. Surface analysis

A combined surface treatment of Acetone degreasing and exposure to UV-light in an ozone-containing atmosphere reduced the value of the contact angle by 43%, from 59° (± 19°), before treatment to 34° (± 6°), after treatment. This value is in accordance with literature and corresponds to a good wettability of the surface [27].

5.2. Quasi-static tensile tests

Fig. 6 and Table 4 present typical load displacement curves for each configuration as well as the average lap shear strength (σ_{LSS}) with standard deviation, derived from the maximum load divided by the overlap area. The displacement depicted in the graph is derived from the mechanical extensometer shown in Fig. 2. Quasi-isotropic layups with 45° and 90° as outermost ply show no appreciable difference in average lap shear strength, while a 0°-layer outside $[(0/45/90/-45)_2]_s$ and the configuration with increased longitudinal bending stiffness $[(45/0/-45/0)_2]_s$ have significantly higher values of average lap shear strength. The 0°-outside configuration shows 46% and the stiffened configuration 98% increase in average lap shear strength in comparison with the reference layup $[(45/90/-45/0)_2]_s$.

For all specimen there is a noticeable non-linearity of the load-displacement curve until approximately 0.1 mm of displacement. It is believed that this trend is caused by initial slack in the testing rig at the beginning of the test. When comparing the stiffness of the different load-displacement curves, layup $[(45/0/-45/0)_2]_s$ shows the steepest slope. This is in agreement with a high longitudinal bending stiffness of the adherend – see Table 3. However, this correlation does not specifically apply to the other three layups, which show almost the same slope. For example, layup $[(0/45/90/-45)_2]_s$ has a 83% higher longitudinal bending stiffness compared to $[(45/90/-45/0)_2]_s$, while the joint stiffness is similar between the two.

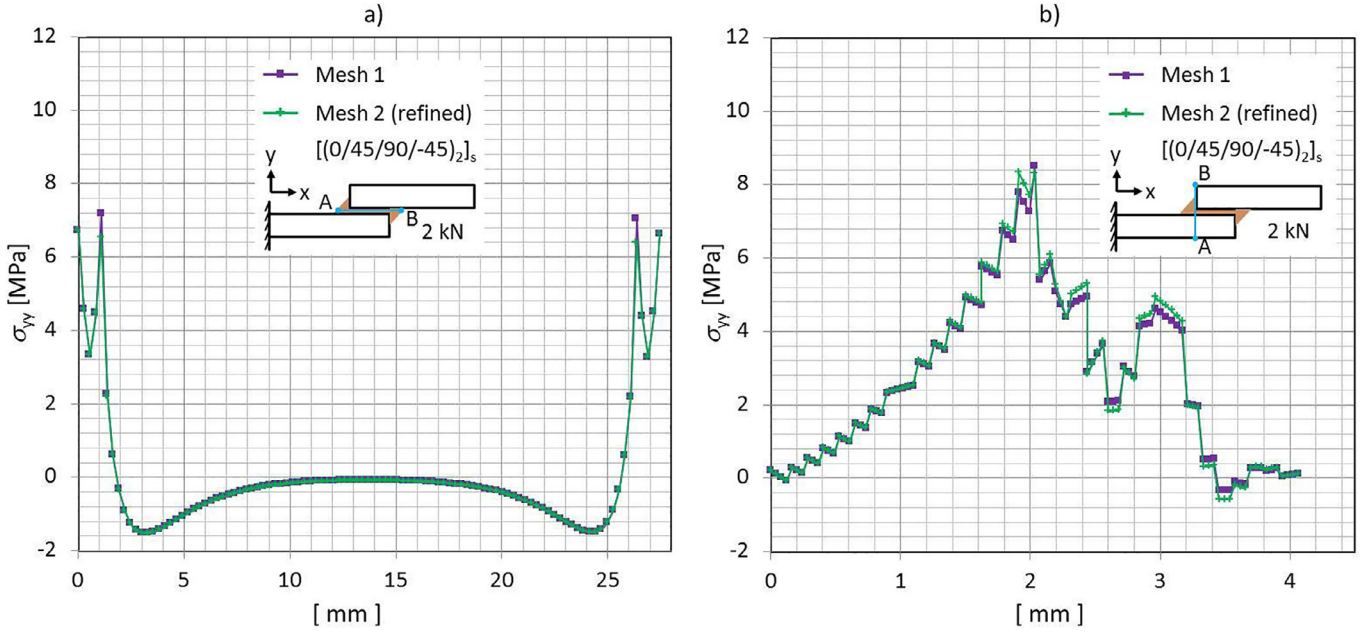

Fig. 5. Mesh convergence study on peel stress (σ_{yy}) distribution along overlap length a) and through bond line thickness b).

5.3. Failure modes

In Fig. 7, the typical fracture surfaces for each layup configuration are illustrated. In Fig. 7c) specimens with the ply angle of 0° adjacent to the bond line failed mostly in the bond line with limited damage on the composite adherends (intra-laminar failure of the 0°-ply). The final fracture surface shows cohesive failure, with yellow shades on either of the adherends fracture surfaces, as well as failure near one of the interfaces, being observed as black surfaces, and switching from one side to the other around the center of the bond line. This failure mode was consistent for all specimens. When the fibre angle of the outermost layer was turned away from 0°, the crack path tended to change from within the bond line into the composite. For the extreme case of a 90° ply angle adjacent to the bond line, the joint failed entirely inside the composite, this being consistent for all specimen – see Fig. 7b). The crack propagated deep into the composite up to the third layer away from the bond line.

For the remaining two configurations with 45° as outside layer, there was a mixed failure mode between the bond line close to the interfaces and failure inside the composite. In case of the reference configuration $[(45/90/-45/0)_2]_s$ in Fig. 7a), the crack propagated up to the third layer of the composite (4th layer visible), while in case of $[(45/0/-45/0)_2]_s$ it reached only the interface between first and second layer – see Fig. 7d). However, this result was not consistent for all 5 specimen in neither of those two configurations. A variation of the area distribution between failure in the adhesive versus failure in the composite, as well as variation in crack depth from 1st up to 4th layer was noticed for the reference layup $[(45/90/-45/0)_2]_s$. The observation matches the larger scatter of measured average lap shear strength in Fig. 6b) for these two configurations. In case of layup $[(45/0/-45/0)_2]_s$, the area distribution between failure in the adhesive versus failure in the composite was similar in all cases, while the crack depth varied between 1st and 2nd layer, reflecting more homogeneous results. It is also interesting to note that for all configurations, the crack has the

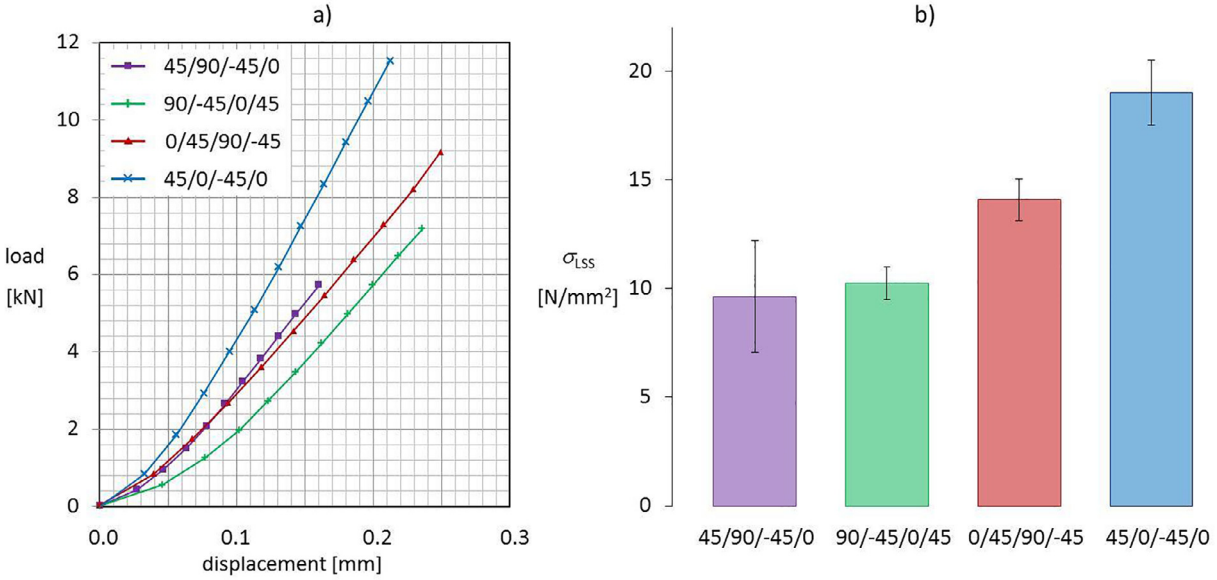

Fig. 6. a) Load-displacement curves, b) average lap shear strength and corresponding standard deviation for different layups.

Table 4
Average lap shear strength, σ_{LSS} (± standard deviation) for different layup configurations.

Layup	$[(45/90/-45/0)_2]_s$	$[(90/-45/0/45)_2]_s$	$[(0/45/90/-45)_2]_s$	$[(45/0/-45/0)_2]_s$
σ_{LSS} [N/mm^2]	9.6 (± 2.5)	10.3 (± 0.8)	14.1 (± 1.0)	19.0 (± 1.5)

tendency to stop propagating inside the composite whenever reaching the first 0°-ply. These observations are in line with Kahn et al. [16]. However, Purimpat et al. [17] observed intra-laminar failure for the case of $[(0/45/90/-45)_2]_s$ inside the adjacent UD-layer rather than cohesive failure in the adhesive.

5.4. Acoustic emission results

Fig. 8 and Table 5 present results from Acoustic Emission monitoring during the tests. In Fig. 8b) the average load for a damage initiation is presented for the four different layup configurations. The values were derived from plotting load versus cumulative acoustic hits of two sensors over time for every specimen. Fig. 8a) shows an example on how these values were derived. The dashed line indicates the load [N] over time [s] and the marked lines represent the cumulative number of acoustic hits over time [s] for one specimen of the layup $[(0/45/90/-45)_2]_s$. A sudden increase of inclination of cumulated hits for both AE-sensors at 53 s indicates the event of a damage initiation at 3500 N for this specimen.

6. Numerical results

6.1. Validation of the numerical model

In order to validate the simulations, the strain distribution measured during test by means of DIC is compared with numerical results. Fig. 9 shows a representative example of the peel strain distribution along the mid-thickness of the bond line. In width direction, the paths is set along the edge of the bond line, where the strains from the DIC are recorded. The values presented correspond to layup $[(0/45/90/-45)_2]_s$ at a reference load of 2.032 kN. This value has been set in order to stay within the area of linear elastic material behaviour before damage initiation.

Overall, the numerical analysis predicts well the experimentally measured strain distribution. The deviation is larger at the bond line tips, where the strains are higher. This might be due to two main reasons: 1) the strain field captured by the camera is representing the strain of the colour coating, that was applied to provide a contrast rich speckle pattern, as common for DIC systems and 2) the method to extract strain values via image correlation software Vic3D 7 by Correlated Solutions, is prone to some inaccuracy when picking the load path, that may not exactly match the ideal location of the numerical model.

Fig. 9 shows an asymmetry in the strains at the region of the tips of the bondline. Since the model contains a perfectly symmetric layup sequence and the design comprises a point symmetry (in 2D) or line symmetry (in 3D, z-direction) around the center of the overlap region, the strain distribution was expected to be symmetric. However, this asymmetry occurs only at the edges, where Fig. 9 is plotted, and it decreases significantly towards the mid width of the specimen.

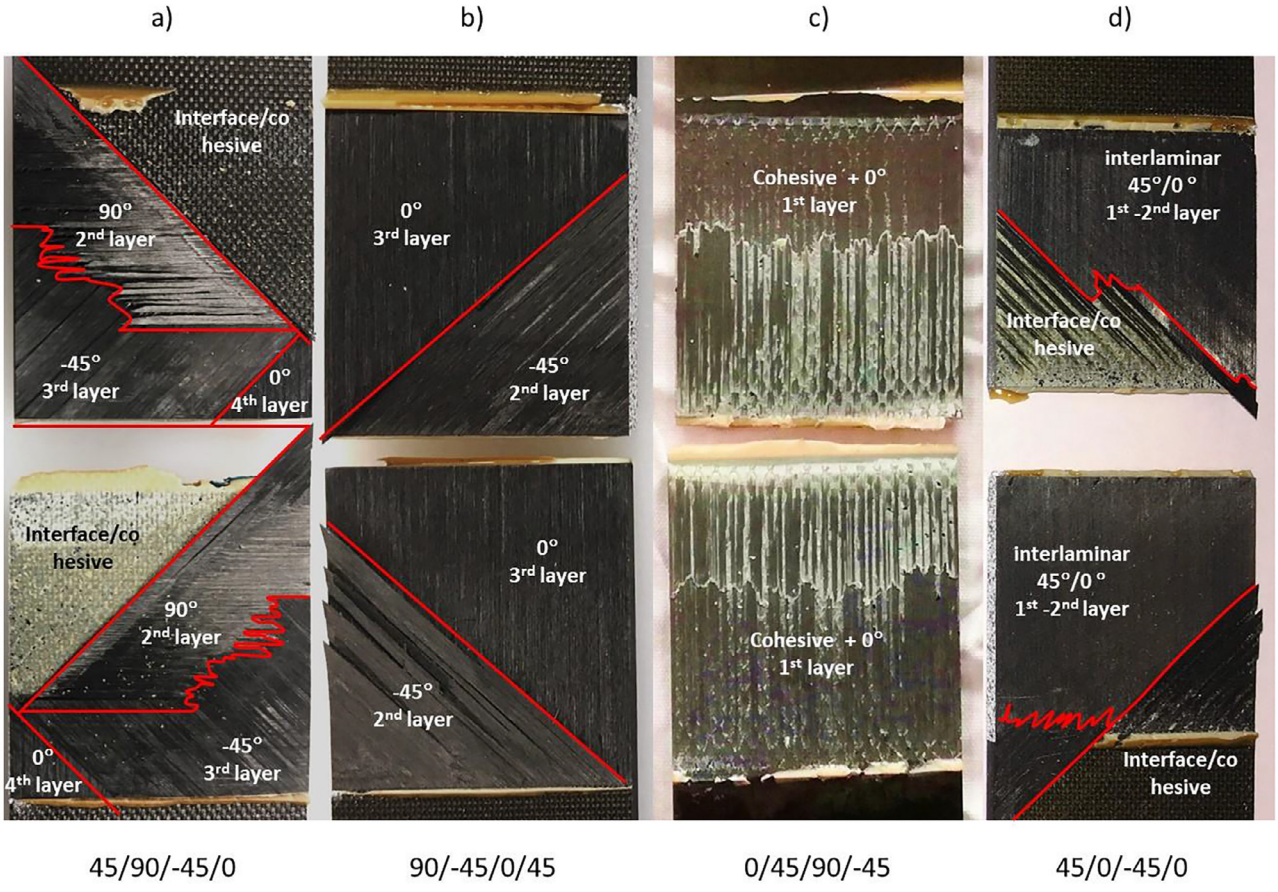

Fig. 7. Typical fracture surfaces for each layup configuration.

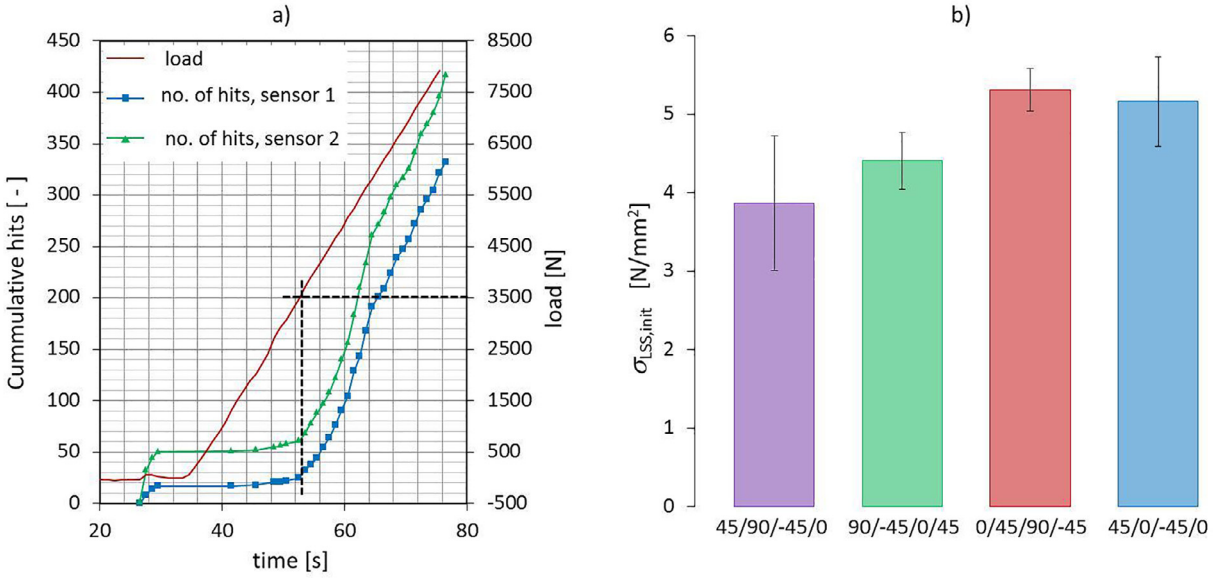

Fig. 8. a) Cumulative acoustic hits vs. load for $[(0/45/90/-45)_2]_s$, b) average lap shear stress (± standard deviation) at damage initiation of different layups.

Table 5
Acoustic Emission results for load and average lap shear stress (± standard deviation) at damage initiation.

Layup	$[(45/90/-45/0)_2]_s$	$[(90/-45/0/45)_2]_s$	$[(0/45/90/-45)_2]_s$	$[(45/0/-45/0)_2]_s$
Load [N]	2540 (± 558)	2870 (± 223)	3440 (± 132)	3280 (± 349)
Average lap shear stress [MPa]	3.87 (± 0.86)	4.41 (± 0.37)	5.31 (± 0.27)	5.16 (± 0.57)

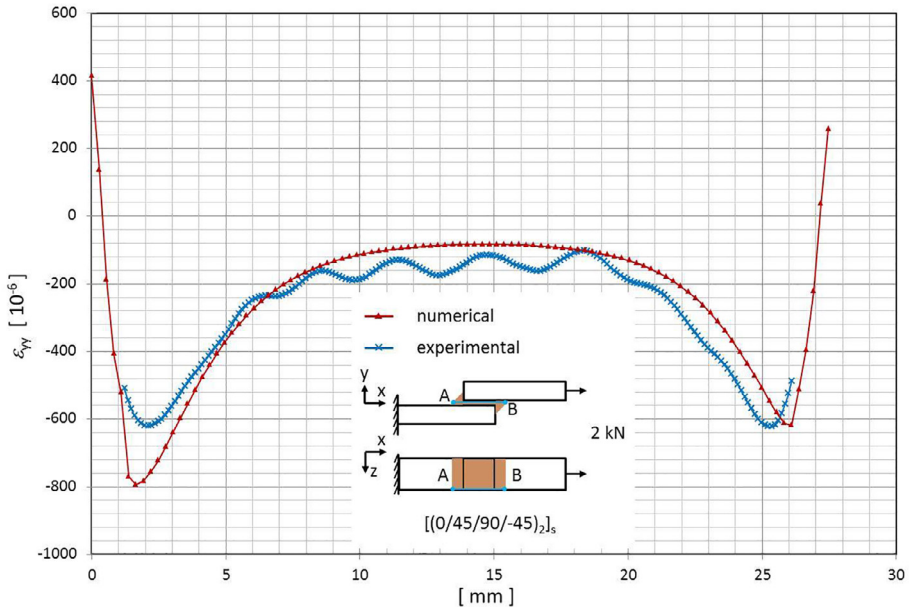

Fig. 9. Peel strain (ε_{yy}) in microstrain [10^{-6}] along the bond line, numerical versus experimental method.

6.2. Stress analysis

The numerical analysis can be further explored to study the stresses around the overlap region. Fig. 10 presents the shear (τ_{xy}) and peel (σ_{yy}) stress distribution along the bond line length for all layup configurations given by the numerical model at a pre-defined load of 2.032 kN, before damage initiation. The plot path is taken at centre position in width direction of the joint and mid-thickness of the bond line.

The comparison of the different layups along the overlap length does not show large deviations in stress level. The plots show the characteristic form for shear and peel stress known from analytical solutions [12]. Only on the shear stresses at the bond line tips, the differences are more visible. The 0/45/90/45 configuration has larger peak shear stresses close to the overlap tips and slightly lower at the mid of the overlap. However, plotting shear (τ_{xy}) and peel (σ_{yy}) stress through the thickness of the overlap, reveals more differences between the layups. In Fig. 11, plots are taken at centre position in width and covers the complete overlap thickness of 4.0625 mm length from bottom to top. Thereafter in Fig. 12, a closer focus is taken onto the near

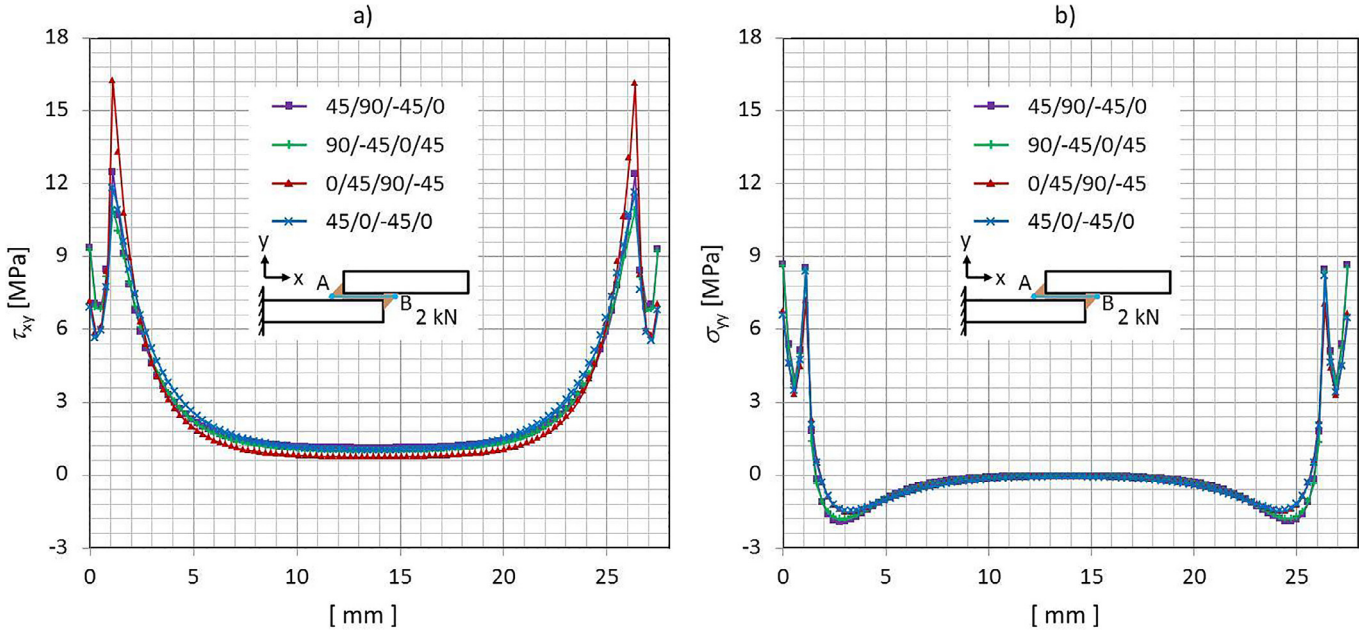

Fig. 10. a) Shear (τ_{xy}), and b) peel (σ_{yy}), stress along the bond line of the joint at centre position in width.

region around the adhesive bond line.

Both stresses contain fairly rough jumps in stress loads at the interfaces between adjacent UD-layers. The peak stresses are in the centre of the plot at the location of the adhesive. There is two interesting findings when analysing these plots. Firstly, when looking into the values for layup $[(0/45/90/-45)_2]_s$ (red line, triangular marker) around the adhesive region, this layup has the highest shear stress value inside the bond line in Fig. 12 a) and at the same time the lowest peel stress, in Fig. 12b). Thus, the ply angle of 0° adjacent to the bond line affects the stress distribution in such a way that the loads are carried mainly by the adhesive layer in shear. The corresponding peel stresses at the adhesive as well as inside the composite laminates are lower for this configuration in comparison with all other configurations – see Fig. 12b). Interestingly, the 0°-outermost configuration is related to mostly cohesive failure, rather than failure inside the composite. This failure pattern fits well with the stress comparison shown in Fig. 12, meaning lower out-of-plane stresses in the composite laminate and higher shear stresses in the adhesive, hence failure mainly in the adhesive.

Secondly, the peel stress plots on the right are more consistent for the different layup configurations, while the shear stress distribution on the left differs more significantly. As peel stresses are out-of-plane, the ply angle does not have a large influence on the peel stress distribution. Therefore, a 0° can carry the same amount of peel stresses as the 45° or 90° – similar out-of-plane stiffness. Contrary to this, for the shear stresses, as an in-plane stress, the fiber angle has a significant influence on its stress distribution. Therefore, the 90° layers are consistently the ones with the lowest shear stresses for all layup configurations, since they have the lowest in plane stiffness.

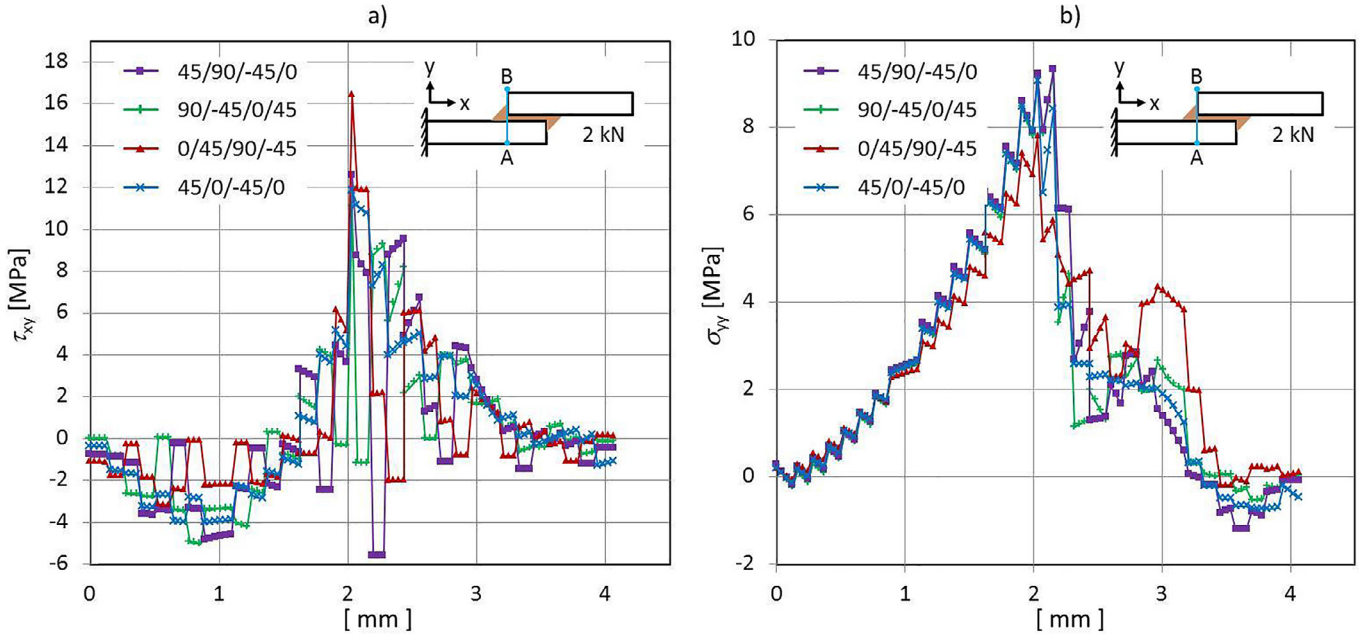

Fig. 11. Shear (τ_{xy}), a) and peel (σ_{yy}), b) stress through the overlap thickness at centre position in width.

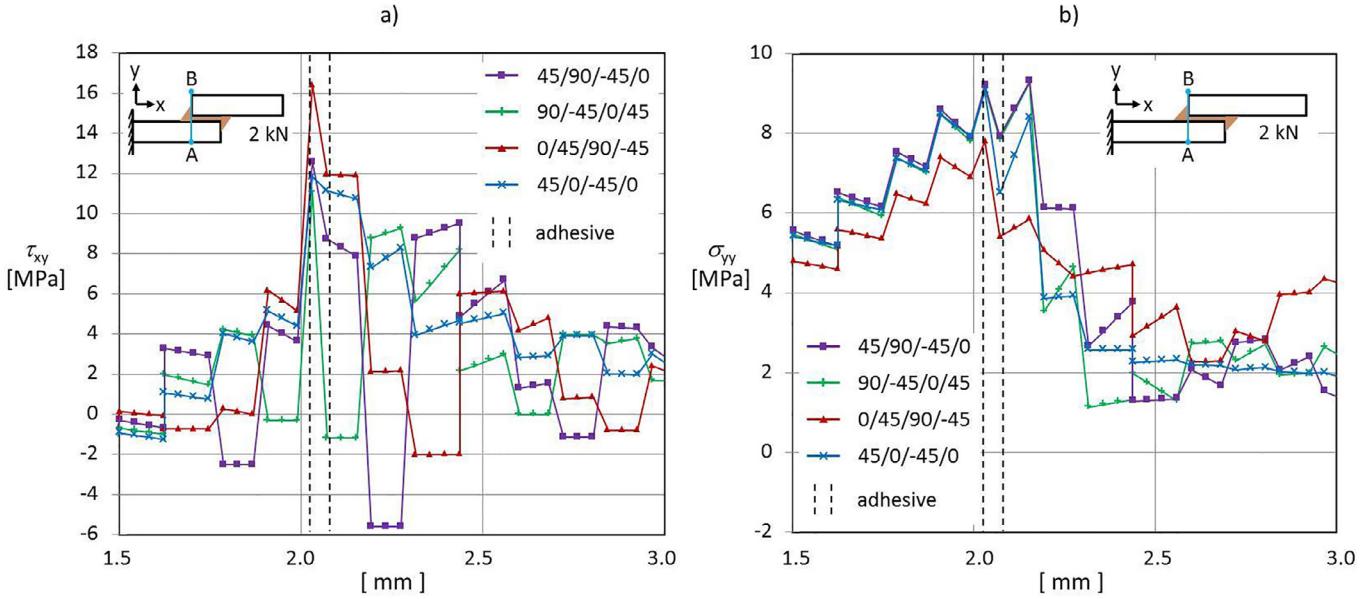

Fig. 12. Shear (τ_{xy}), a) and peel (σ_{yy}), b) stress through the overlap thickness at centre position in width, focussed region around the bond line.

6.3. Damage initiation

The numerical approach to derive the load at damage initiation was established by post-processing the stress tensor for every node. A set of user-defined subroutines was built to contain various failure criteria. As a result of the World-Wide Failure Exercise (WWFE) I and II [28,29], one can find a variety of applicable failure criteria, based on continuum damage mechanics, for composite structures under different two- or three-dimensional stress states. The benchmark results also reveal that not every failure theory can conclusively predict every load case and failure pattern [30]. On the other hand, the unsymmetrical 3D-stress state inside a single overlap has not been covered by any of the WWFE test cases. Therefore, to ensure reliable results, it was decided to use several failure criteria for both the composite and the adhesive in order to understand which criterion fits the best to this specific load case. For a failure inside the composite, the Hashin [31,32], Puck [33–35] and a 3D-invariant based criterion of Camanho et. al. [36] were used. All three criteria distinguish between fibre and matrix failure. For the adhesive, the von Mises and the quadratic Drucker-Prager yield criterion were used. In the later, the study follows the approach of L.F.M. da Silva et al. [37,38], where the yield criterion can be expressed as

$$aq^b - p = p_t \tag{2}$$

The terms that appear in Equation (2) are defined as

$$a = \frac{1}{3(\beta - 1)\sigma_{yt}} \tag{3}$$

$$q = \sqrt{\frac{1}{2}[(\sigma_1 - \sigma_2)^2 + (\sigma_2 - \sigma_3)^2 + (\sigma_3 - \sigma_1)^2]} \tag{4}$$

$$b = 2$$

$$p = -\frac{1}{3}(\sigma_1 + \sigma_2 + \sigma_3) \tag{5}$$

$$p_t = \frac{\beta\sigma_{yt}}{3(\beta - 1)} \tag{6}$$

with b as the exponent parameter, σ_{yt} for the adhesive's yield stress in tension, β representing the ratio of yield stress in compression to the yield stress in tension and σ_1, σ_2 and σ_3 being the principal stresses at the element nodes. Those stress values were linearly extrapolated from the integration points, according to the given element type C3D8. In this study, there were no experimental values available for the compressive yield stress of the chosen adhesive Hysol® EA 9695™ 050K AERO. The β-value was chosen 1.45, based on values found in literature for adhesives with comparable Young's modulus and yield strength [4,21,37].

For the failure criteria of the composites, it is important to note that the strength of a single UD-layer inside a stacking sequence varies with respect to its ply thickness and position within the sequence. This in-situ effect is incorporated, following recent work of Camanho et al. [39]. The UD-properties in comparison with their elevated in-situ representative are shown in Table 6.

The occurrence of damage initiation was determined, once the specific failure criterion indicates that at least one node reaches failure. Values at which damage initiation is indicated in the numerical model were then compared with the loads indicated by the Acoustic Emission during the experiments. Fig. 13 and Table 7 illustrate the comparison of experimental AE-results versus the numerical approach in terms of average la shear stress at damage initiation.

Considering the mechanical behaviour of single lap joints under tension [1,12] and looking to the failure modes presented in Fig. 7, matrix tensile failure is the dominant failure mode within the composite laminate. After the index values for all different failure modes were checked, matrix tension values were identified as most critical. Hence the index values, presented in Fig. 13 and Table 7, solely represent this case. For the first two laminates, $[(45/90/-45/0)_2]_s$ and $[(90/-45/0/45)_2]_s$ the criteria indicate failure within adhesive and in the composite at loads close to the experimental results. There is a tendency though, that in both layups the damage initiates inside the adhesive (except for Hashin's criterion). For the two stronger layups, $[(0/45/90/-45)_2]_s$

Table 6
UD versus in-situ properties for a 16-ply layup of Hexply® 6376C-HTS(12K)-5-35%

	UD properties [MPa]		In situ properties [MPa]	
In-plane shear strength	s_L	104	s_L^{is}	126
Transverse shear strength	s_T	35	s_T^{is}	42
Transverse tensile strength	y_T	102	y_T^{is}	162
Transverse biaxial tensile strength	y_{BT}	63	y_{BT}^{is}	110
Transverse compressive strength	y_C	−255	y_C^{is}	−296

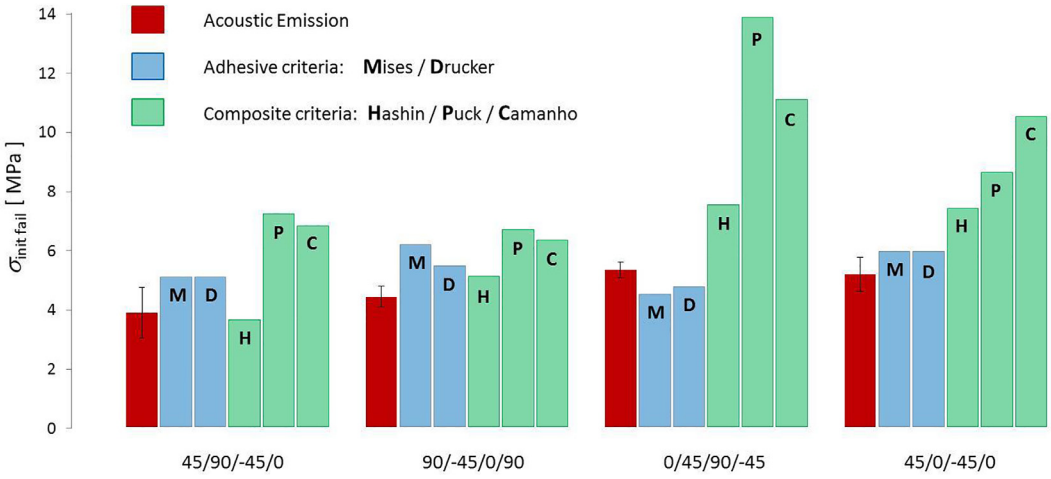

Fig. 13. Average lap shear stress at damage initiation: experimental versus numerical results.

and $[(45/0/-45/0)_2]_s$ damage initiation at the composite adherents is generally indicated at significantly higher loads than for the adhesive. The adhesive failure criteria are in overall agreement with the experimental results. For all four layups, damage initiation tends to appear in the adhesive. However the loads of failure initiation of the adhesive and of the composite tend to get closer for the configuration of $[(90/45/0/45)_2]_s$ and further away for the $[(0/45/90/45)_2]_s$. The fact that the load for damage initiation in the composite is significantly higher than in the adhesive for the layups $[(0/45/90/-45)_2]_s$ and $[(45/0/-45/0)_2]_s$, in comparison with the layups $[(45/90/-45/0)_2]_s$ and $[(90/-45/0/45)_2]_s$, shows that a crack is less likely to grow inside the composite in the two former layups than in the two later layups. This is very much in agreement with the fracture surfaces presented in Fig. 7, since for the layups $[(45/90/-45/0)_2]_s$ and $[(90/-45/0/45)_2]_s$ the damage grows further inside the composite than for the layups $[(0/45/90/-45)_2]_s$ and $[(45/0/-45/0)_2]_s$. Layups $[(0/45/90/-45)_2]_s$ and $[(45/0/-45/0)_2]_s$ show a larger scatter between the composite criteria with no visible trend. The failure indices for the criteria of Puck and Camanho include the in-situ effect for material allowables, whereas the original UD-properties were used for Hashin's criterion. With respect to the SLJ-design and materials depicted by this study, there is no clear tendency which of the composite criteria is more applicable, since there is no general trend for all layups studied, whereas both criteria for failure inside the adhesive, Mises and Drucker-Pragel, indicate similar values that match well with the experimentally observed.

Fig. 14 illustrates the location of failure according to each criterion. The location was determined from the node coordinates given by the Abaqus input-file. All criteria consistently indicate failure in the region around the bond line tip of the non-free adherend side. The location may arbitrarily switch from the left to the right tip since stresses are fairly similar in both overlap tips. Looking through the thickness of the overlap, the adhesive tends to fail at the interface with the first UD-layer for all layups. In case of composite failure, the location differs. Depending on the layup, failure in the composite tends to initiate at the interface of that UD-layer with the lowest longitudinal bending stiffness, meaning near the 90°-layer. This result does generally correspond to the observations of fracture surfaces in Fig. 7. However, the final fracture surface at maximum load is a different state and cannot be taken as direct guideline to predict an initial failure mechanism.

7. Discussion

Fig. 15 summarizes the experimental results. It presents the average lap shear strength (σ_{LSS}, based on the maximum load), the AE-based average lap-shear stress at damage initiation (σ_{init}), the final fracture surfaces and the equivalent longitudinal bending stiffness for all configurations. Quasi-isotropic layups with 45° and 90° as outermost ply show similar average lap shear strength, while a 0°-layer outside and the configuration with increased longitudinal bending stiffness have significantly higher values. The AE-based stresses, where damage initiation is estimated, are significantly lower (less than 50%) than average lap shear strength (σ_{LSS}) in all cases. This difference indicates that there is still a remarkable portion of residual tensile strength for composite bonded joints after damage initiation.

7.1. Effect of bending stiffness of the laminates

From the layups investigated, there is clearly two groups in terms of bending stiffness of the laminate adherends: the group with lower bending stiffness, the first two layups $[(45/90/-45/0)_2]_s$ and $[(90/-45/0/90)_2]_s$, and the group with higher bending stiffness, the two last layups $[(45/0/-45/0)_2]_s$ and $[(0/-45/90/45)_2]_s$. In terms of damage initiation, these groups can be distinguished as: lower stiffness leads to lower loads at damage initiation and vice versa, which has been observed both experimentally and numerically. Numerical simulations indicate that there is a tendency for damage to initiate in the adhesive bond line. This is in fact in accordance with earlier studies [12–14], correlating strength of SLJs only to the stress analysis and adhesive

Table 7
Average lap shear strength (± standard deviation) versus stress at damage initiation: Experimental (EXP) and numerical (NUM) approach with values in [N/mm^2]

Layup	$[(45/90/-45/0)_2]_s$	$[(90/-45/0/45)_2]_s$	$[(0/45/90/-45)_2]_s$	$[(45/0/-45/0)_2]_s$
σ_{LSS}-EXP	9.6 (± 2.6)	10.3 (± 0.7)	14.1 (± 1.0)	19.0 (± 1.5)
σ_{1st_AE}-EXP	3.9 (± 0.9)	4.4 (± 0.4)	5.3 (± 0.3)	5.2 (± 0.6)
σ_{1st_Mises}-NUM	5.1	6.2	4.5	5.9
$\sigma_{1st\_Drucker}$-NUM	5.1	5.4	4.8	5.9
σ_{1st_Hashin}-NUM	3.6	5.9	7.5	7.4
σ_{1st_Puck}-NUM	7.2	6.7	13.8	8.6
$\sigma_{1st\_Camanho}$-NUM	6.8	6.3	11.6	10.5

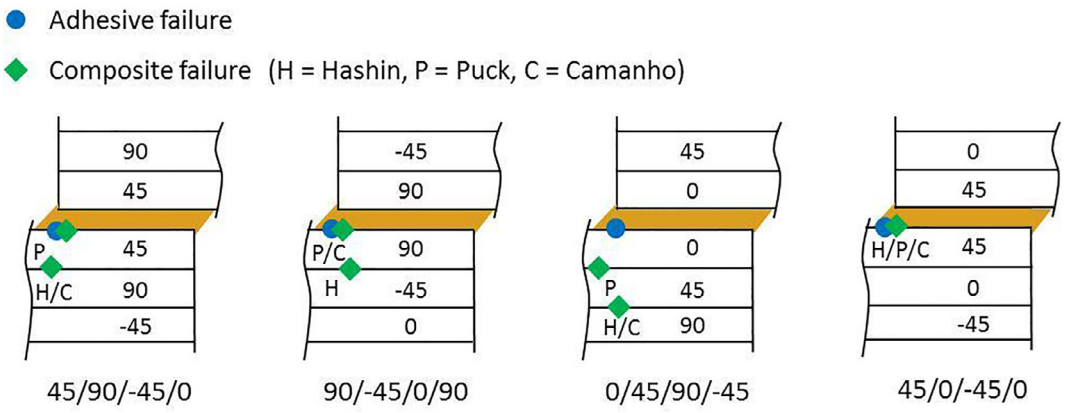

Fig. 14. Location of damage initiation due to FEM-analysis.

failure. However, when we look to the maximum load carried by the joints – by means of average lap shear strength, this trend does not entirely apply. It is noticeable the layups $[(45/0/-45/0)_2]_s$ and $[(0/-45/90/45)_2]_s$, with similar bending stiffness, have similar loads at damage initiation but a difference of 35% in average lap shear strength (σ_{LSS}). This means that for the same bending stiffness if changing the stacking sequence such that the final failure progresses inside the composite adherend, i.e., from $[(0/-45/90/45)_2]_s$, – damage inside the adhesive, to $[(45/0/-45/0)_2]_s$ – damage inside the composite, the average lap shear strength increases.

Taking into account the relative bending stiffness of each layup configuration, it can then be concluded that increasing the bending stiffness leads to an increase of the joint strength associated with damage initiation. After crack initiation, damage progression inside the composite yields to higher ultimate failure load than one inside the adhesive. This conclusion draws the limits of previous recommendations made in literature to increase bending stiffness to increase joint strength up to damage initiation. If the aim is to increase the maximum lap shear strength at failure, this recommendation is no longer valid.

7.2. Effect of the angle of the composite layer in contact with the adhesive

7.2.1. Effect on the failure mode

Based on the observations of the fracture surfaces, the final failure mode is influenced by the orientation of the outermost lamina, in such a way that a 0° ply in contact with the adhesive will favour failure inside the adhesive and larger angles will favour failure to grow inside the composite. This is in agreement with previous work of Aydin [14], Khan et al. [16], and Purimpat et al. [17] and can be explained with the peel stress (σ_{yy}) and shear stress (τ_{xy}) distribution through the overlap thickness shown in Figs. 11 and 12. Now, the question can be replied, why the appearance of a 0°-ply orientation always prevents a crack to grow further into the composite. On the one hand, layup $[(0/-45/90/45)_2]_s$ has the highest shear stress level inside the bond line, with a distinct drop towards the adherends. In addition, this layup has the lowest peak stress in peel at the adhesive, again with a rapid decrease towards the composite. Stresses are focussed on the very narrow area of the bond line and drop significantly when reaching the composite adherend. This results in the joint to fail cohesively inside the adhesive. On the other hand, for the remaining configurations with larger ply-angles in contact with the adhesive, the peel stresses are high in the adhesive and in the composite adherend. This favours failure to propagated inside the composite, as observed in the final fracture surfaces.

7.2.2. Effect on the average lap shear strength – final failure

The results shown in Figs. 6 and 7 indicate that, cohesive failure does not necessarily lead to the higher lap shear strength at final failure than failure inside the composite. In fact for laminates with similar bending stiffness, such as $[(45/0/-45/0)_2]_s$ and $[(0/-45/90/45)_2]_s$, a failure inside the composite in the former leads to higher lap shear strength than cohesive failure inside the adhesive. It can be concluded that, for the same bending stiffness, larger ply-angles in contact with the adhesive will increase the lap shear strength of the SJL at final failure. This results are in agreement with the previous of work of Purimpat et al. [17]. However they are both in disagreement with the previous work of Khan et al [16] where is concluded, that highest maximum load at quasi-static testing is reached by the configuration with cohesive failure inside the adhesive. As there were not the exact same layup configurations investigated, results may differ.

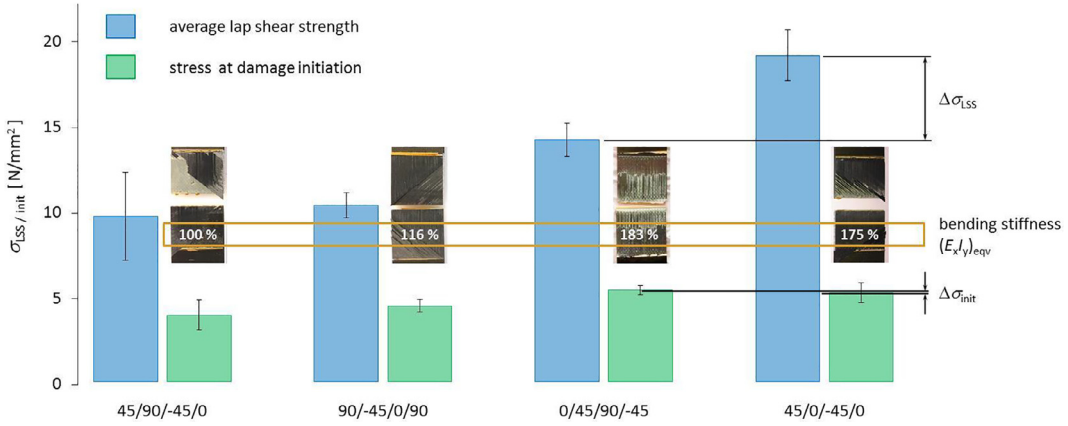

Fig. 15. Average lap shear strength (± standard deviation) at maximum load vs. damage initiation in respect to bending stiffness.

8. Conclusions

This study aims to understand the effect of the composite layup on the damage initiation and final failure of composite bonded single lap joints under quasi-static tensile loading. Four different configurations were studied, with the quasi-isotropic stacking sequence $[(45/90/-45/0)_2]_s$ as the reference layup. Three other layups ($[(90/-45/0/45)_2]_s$, $[(0/-45/0/45)_2]_s$ and $[(45/0/-45/0/45)_2]_s$) were tested in which the angle of the layer in contact with the adhesive ($[(90/-45/0/45)_2]_s$, $[(0/-45/0/45)_2]_s$) and the longitudinal bending stiffness of the adherends ($[(45/0/-45/0/45)_2]_s$) were varied. Tests were monitored to identify damage initiation loads, as well as maximum loads. FE-analysis were performed to numerically simulate the experimental tests up to damage initiation. From the analysis of the results the following conclusions can be drawn:

- An increase of the in-plane longitudinal bending stiffness of the laminate adherends postpones damage initiation. For all layup configurations, damage tends to initiate in the bond line and therefore, a stiffer laminate decreases the stress field in the bond line region and increases the load up to damage initiation. However, this relation between stiffness and strength is no longer valid on maximum lap shear strength at failure load.
- The damage progression is influenced by the orientation of the outermost lamina such that, a fiber orientation towards 0° causes the crack to propagate cohesively within the adhesive bond line while as the ply angle increases, the crack tends to propagate further inside the composite. This is related with the fact that, a layup with 0° adjacent to the adhesive interface leads to an increase in the shear stresses inside the adhesive but lower peel stresses inside the composite layup, while a layup with larger ply angles in contact with the adhesive increases the peel stresses in the adhesive and in the neighbouring composite layup.
- The ply angle has a larger influence on the (in-plane) shear stresses than on the (out-of-plane) peel stresses.
- For similar adherend bending stiffness, larger ply-angles in contact with the adhesive will increase the lap shear strength of the SJL at final failure, because they promote crack propagation inside the composite rather than inside the adhesive.
- There is a clear distinction between the layup effect properties in the damage initiation and final failure of the SLJ. Therefore, an optimized layup might be very different, if the goal is to postpone damage initiation or final failure.
- Finally, a quasi-isotropic layup may not be the best choice, in terms of tensile joint strength, based on the linear-elastic/plastic approach of this study. The findings of this study could then be the basis for a further optimization process of the layup beyond common ply angles.

Acknowledgement

This work has been funded by the Netherlands Organisation for Scientific Research (NWO), project number 14366.

Data availability

The data required to reproduce these findings are available to download from http://doi.org/10.4121/uuid:8a51631a-a18e-4737-9757-6d325d8733c0.

References

[1] Godwin EW, Matthews FL. Review of the strength of joints in fibre-reinforced plastics: part 2 adhesively bonded joints. Composites 1982;13(1):29–37.
[2] Adams RD. Strength predictions for lap joints, especially with composite adherends. A review. J Adhes 1989;30(1–4):219–42.
[3] Teixeira de Freitas S, Sinke J. Adhesion properties of bonded composite-to-Aluminium joints using peel tests. J Adhes 2014;90:511–25.
[4] Teixeira de Freitas S, Sinke J. Failure analysis of adhesively-bonded skin-to-stiffener joints: Metal–metal vs. composite–metal. Eng Failure Anal 2015;56:2–13.
[5] Kruse T, Koerwien T, Ruzek R. Fatigue behaviour and damage tolerant design of composite bonded joints for aerospace application. 17th European Conference on Composite Materials, Munich, Germany. 2016.
[6] Peeters D, Abdalla M. Design guidelines in nonconventional composite laminate optimization. J Aircraft 2017;54(4):1454–64.
[7] Lopes CS, Camanho PP, Gürdal Z, Maimí P, González EV. Low velocity impact damage on dispersed stacking sequence laminates. Part II: numerical simulations. Compos Sci Technol 2009;69(7–8):937–47.
[8] Muc A, Gurba W. Genetic algorithms and finite element analysis in optimization of composite structures. J Compos Struct 2001;54(2–3):275–81.
[9] Sebaey TA, González EV, Lopes CS, Blanco N, Costa J. Damage resistance and damage tolerance of dispersed CFRP laminates: design and optimization. J Compos Struct 2013;95:569–76.
[10] Shang X, Marques EAS, Machado JJM, Carbas RJC, Jiang D, da Silva LFM. A strategy to reduce delamination of adhesive joints with composite substrates. Proc Inst Mech Eng Part L. Special Issue MDA2018. DOI: 10.1177/1464420718805712.
[11] Schollerer MJ, Kosmann J, Völkerink O, Holzhüter D, Hühne C. Surface toughening – a concept to decrease stress peaks in bonded joints. J Adhes 2018;94(14). https://doi.org/10.1080/00218464.2018.1555041.
[12] Hart-Smith LJ. Adhesive bonded single-lap joints Long Beach, CA, United States: Douglas Aircraft Co., Inc.; 1973. Technical report NASA CR 112236.
[13] Renton WJ, Vinson JR. The efficient design of adhesive bonded joints. J Adhes 1975;7:175–93.
[14] Aydin MD. 3-D nonlinear stress analysis on adhesively bonded single lap composite joints with different ply stacking sequences. J Adhes 2008;84:15–36.
[15] Özel A, Yazici B, Akpinar S, Aydin MD, Temiz S. A study on the strength of adhesively bonded joints with different adherends. Compos B 2014;62:167–74.
[16] Khan MA, Hamar CO, Aglietti GS, Crocombe AD, Viquerat AD. Development of rules for the design of composite bonded joints. 11th European Adhesion Conference, Glasgow, United Kingdom. 2016. p. 331–4.
[17] Purimpat S, Shahram RJ, Shahram A. Effect of fibre angle orientation on a laminated composite single-lap adhesive joint. J Adv Compos Mater 2013;22(3):139–49.
[18] Meneghetti G, Quaresimin M, Ricotta M. Influence of the interface ply orientation on the fatigue behaviour of bonded joints in composite materials. Int J Fatigue 2010;32(1):82–93.
[19] Meneghetti G, Quaresimin M, Ricotta M. Damage mechanisms in composite bonded joints under fatigue loading. Compos B 2012;43:210–20.
[20] Material datasheet. A75-T-2-0123-1-1. Airbus material-handbook structure; 2014.
[21] Teixeira de Freitas S, Sinke J. Failure analysis of adhesively-bonded metal-skin-to-composite-stiffener: effect of temperature and cyclic loading. J Compos Struct 2017;166:27–37.
[22] ASTM D5868 -01. Standard test method for lap shear adhesion for fiber reinforced plastic (FRP) bonding; 2014.
[23] Kaw K. Mechanics of composite materials. 2nd ed. Boca Raton, FL: Taylor & Francis; 2006.
[24] Holtmannspoetter J, Czarnecki JV, Wetzel M, Dolderer D, Eisenschink C. The use of peel ply as a method to create reproduceable but contaminated surfaces for structural adhesive bonding of carbon fiber reinforced plastics. J Adhes 2013;89(2):96–110.
[25] Ultraviolet-ozone surface treatment. Three bond technical news; 1987.
[26] Poulis JA. Small cylindrical adhesive bonds [Ph.D. thesis]. Technical University Delft: The Netherlands; 1993. pp. 39–62. ISBN-90-370-0082-7.
[27] Teixeira de Freitas S, Zarouchas D, Poulis JA. The use of acoustic emission and composite peel tests to detect weak adhesion in composite structures. J Adhes 2018;94:743–66.
[28] Hinton MJ, Kaddour AS. The background to the second world-wide failure exercise. J Compos Mater 2012;46:19–20.
[29] Hinton MJ, Kaddour AS. The background to Part B of the second world-wide failure exercise: evaluation of theories for predicting failure in polymer composite laminates under three-dimensional states of stress. J Compos Mater 2013;47:6–7.
[30] van Dongen B, van Oostrum A, Zarouchas D. A blended continuum damage and fracture mechanics method for progressive damage analysis of composite structures using XFEM. Compos Struct 2018;184:512–22.
[31] Hashin Z. Failure criteria for unidirectional fiber composites. J Appl Mech 1980;47:329–34.
[32] Kress G. Examination of Hashin's failure criteria for Part B of the second world-wide failure exercise: comparison with test data. J Compos Mater 2013;47(6–7):867–91.
[33] Puck A, Schuermann H. Failure analysis of FRP laminates by means of physically based phenomenological models. J Compos Sci Technol 1998;58:1045–67.
[34] Puck A, Kopp J, Knops M. Guidelines for the determination of the parameters in Puck's action plane strength criterion. J Compos Sci Technol 2002;62:371–8.
[35] Deuschle M, Puck A. Application of the Puck failure theory for fibre-reinforced composites under three-dimensional stress: comparison with experimental results. J Compos Mater 2013;47(6–7):827–46.
[36] Camanho PP, Arteiro A, Melro AR, Catalanotti G, Vogler M. Three-dimensional invariant-based failure criteria for fibre-reinforced composites. Int J Solids Struct 2015;55:92–107.
[37] da Silva LFM, Rodrigues TNSS, Figueiredo MAV, de Moura MFSF, Chousal JAG. Effect of adhesive type and thickness on the lap shear strength. J Adhes 2007;82:1091–115.
[38] Drucker DC, Prager W. Soil mechanics and plastic analysis or limit design. Quart Appl Math 1952;10:157–65.
[39] Camanho PP, Davila CG, Pinho ST, Iannucci L, Robinson P. Prediction of in situ strengths and matrix cracking in composites under transverse tension and in-plane shear. Compos A 2006;37:165–76.